

Induced photofission and spallation on the pre-actinide nucleus

^{181}Ta .

A. Deppman,^{*} G. S. Karapetyan,[†] V. Guimarães,[‡] and C. Gonzales[§]

*Instituto de Fisica, Universidade de São Paulo,
P. O. Box 66318, 05315-970 São Paulo, SP, Brazil*

A. R. Balabekyan[¶]

*Yerevan State University, Faculty of Physics,
Alex Manoogian 1, Yerevan 0025, Armenia*

N. A. Demekhina^{**}

*Yerevan Physics Institute, Alikhanyan Brothers 2, Yerevan 0036, Armenia
Joint Institute for Nuclear Research (JINR),
Flerov Laboratory of Nuclear Reactions (LNR),
Joliot-Curie 6, Dubna 141980, Moscow region Russia*

Abstract

A study of photofission on ^{181}Ta nucleus induced by bremsstrahlung photons with endpoint energies of 50 and 3500 MeV has been performed. The fission yields have been measured by using the induced-activity method in an off-line analysis. The absolute photofission cross sections for the tantalum target at 50 and 3500 MeV are found to be $5.4 \pm 1.1 \mu\text{b}$ and $0.77 \pm 0.11 \text{ mb}$, respectively, and the corresponding deduced fissilities are $(0.23 \pm 0.05) \times 10^{-3}$ and $(2.9 \pm 0.9) \times 10^{-3}$. Mass- and charge-yield distributions were derived from the data. The results were compared with the simulated results from CRISP code for multi-modal fission by assuming symmetrical fission mode.

PACS numbers: 24.75.+i, 25.85.Jg

^{*}Electronic address: deppman@if.usp.br

[†]Electronic address: ayvgay@if.usp.br

[‡]Electronic address: valdirg@if.usp.br

[§]Electronic address: cgonzaleslorenzo@gmail.com

[¶]Electronic address: balabekyan@ysu.am

**Electronic address: demekhina@nrmil.jinr.ru

I. INTRODUCTION

Induced fission has been studied over the years by a wide variety of projectiles and energy range. The information obtained from these experiments encompassed different characteristics of the fissioning system. Photofission is one of the most powerful tools for studying the fission process because of the well known spin selectivity of the excitation and the absence of the Coulomb barrier. Photons interact with nuclei by the quasideuteron mechanism and meson production. The main experimental problem in photofission studies is the lack of an intense source of monochromatic photon beam. Therefore, a large amount of photofission mass-yield distributions has been measured with bremsstrahlung spectra with a continuous energy distribution in the energy range of 300 to 1800 MeV [1–4]. Related to photofission on heavy nuclei, many works have been performed, with monochromatic photons at intermediate and high-energy regime, using different experimental techniques [5–9]. In these experiments, the photofission cross sections, and related fissility (the ratio of fission cross section to total nuclear photoabsorption cross section), were determined for pre-actinide targets with fissility parameter $Z^2/A < 31.6$. At low photon incident energies (≤ 30 MeV), pre-actinide nuclei do not exhibit the resonance pattern characteristic of the giant resonance excitation [2, 7]. Although very important for very heavy elements, giant-resonance fission contribution is unimportant for elements with atomic number $Z < 83$ because of the high fission thresholds (22-27 MeV [5]) and small values of the parameter Z^2/A . For nuclei with mass number $A < 210$ the trends of the photofission cross section show, conversely, an increase of several orders of magnitude, for incident energy from the fission threshold (~ 20 -30 MeV) up to about 200 MeV [7].

Mass-yield distribution for fission of different nuclear systems, which may exhibit symmetric and asymmetric modes and transition between them, is of particular interest in the investigation of the fission process. It is well known that mass distributions for actinide fission, induced by different projectiles and at intermediate energies, exhibit both symmetric and asymmetric modes. These fission modes can successfully be represented by Gaussian curves, and less than five Gaussian curves were adequate to describe mass distribution of induced fission on pre-actinides and higher actinides nuclei, where increasingly symmetric fission is observed [10]. It is well known that fission is predominantly symmetric for pre-actinides with $A \leq 227$, since the targets are above the Businaro-Gallone point [11].

Actually, symmetric fission components have been observed in all photofission experiments with pre-actinides, but most of the time a quantitative comparison between each other is difficult due to different methods used in the analysis.

The absence of a reliable theoretical model to predict fission yields, as well as the need for more experimental data, motivated us to investigate photofission processes of pre-actinide nuclei. The essential goal of this paper is to present the measurement of the formation cross sections of fission fragments of ^{181}Ta nucleus induced by bremsstrahlung photons with endpoint energies of 50 and 3500 MeV. In this experiment the total fission cross sections for both energies were derived from the experimental yields of fission fragments measured using off-line induced-activity method. Investigation of photofission on such nucleus is also of importance for practical applications such as astrophysics, medicine, accelerator technology and nuclear waste transmutation.

Present experimental results for the fission process of the ^{181}Ta nucleus were compared with calculations by CRISP code based on the multi-modal fission approach [12]. This comparison allowed us to extract information on the reaction mechanism related to fission and spallation processes.

II. EXPERIMENTAL PROCEDURE

The data for the photofission cross sections of ^{181}Ta were obtained using bremsstrahlung photon radiation. The bremsstrahlung photon with endpoint energies of 3500 and 50 MeV were obtained by using electrons of the Yerevan electron synchrotron and a linear accelerator of the injector type, respectively. The electrons were converted into bremsstrahlung-photon beam by means of tungsten converter of about $300\ \mu\text{m}$ (about 0.1 radiation-length units) in thickness. The reaction chamber at the injector was arranged immediately after the converter. A beam-cleaning and beam-formation system consisted of a set of collimators and it was used in the irradiation with high-energy photon beam. The high-energy photon beam passed through the first collimator, $3 \times 3\ \text{mm}^2$ in dimension, and a cleaning magnet, which removed the charged component. The second collimator, $10 \times 10\ \text{mm}^2$ in dimension, was responsible for removing the beam halo. The photon-beam intensity was measured by a Wilson-type quantometer giving an average of $\sim 10^{11}$ equivalent quanta per second (eq. q. s^{-1}) at 3500 MeV and $\sim 10^9$ equivalent quanta per second (eq. q. s^{-1}) at 50 MeV.

The photon beam intensities were evaluated from the monitor reactions $^{27}\text{Al}(\gamma, 2\text{pn})^{24}\text{Na}$ and $^{65}\text{Cu}(\gamma, \text{n})^{64}\text{Cu}$, with known cross-sections [13, 14]. The 0.164g ^{181}Ta target, with natural isotopic composition (99,98799%) and 0.0487 mm in thickness, was irradiated for 196 min and 43 min with the photon beam with endpoint energies 3500 MeV and 50 MeV, respectively.

The yields of radioactive fragments were measured in an off-line analysis using a high-purity germanium (HpGe) detector (80 cm³) with a resolution of about 0.2% at the ^{60}Co γ -transition energy of 1332 keV. The γ -spectrometer detection efficiencies for four different target-detector distances, namely 0.0, 22.0, 7.0, and 25.0 cm, were determined by using the standard radiation sources of ^{22}Na , ^{54}Mn , $^{57,60}\text{Co}$, and ^{137}Cs . To obtain the energy dependence of the detector efficiency for energies above 1500 keV, we used also the data from the $^{27}\text{Al}(\gamma, 2\text{pn})^{24}\text{Na}$ reaction ($E_\gamma = 2754$ keV). The final energy dependence of the HpGe-detector efficiency was obtained with a precision of 10%. Measurements of the γ -spectra started about 120 minutes after the completion of the irradiation and lasted a year. The identification of the reaction products, and the determination of their production cross section, were performed considering the half-lives, energies and intensities of the γ -transition of the radioactive fragments.

The fragment production yields are considered direct and independent (I) in the absence of a parent isotope contribution (which may give a contribution via β^\pm -decays) and are determined by the following equation:

$$Y = \frac{\Delta N \lambda}{N_p N_n k \epsilon \eta (1 - \exp(-\lambda t_1)) \exp(-\lambda t_2) (1 - \exp(-\lambda t_3))}, \quad (1)$$

where Y denotes the yields of the reaction fragment production; ΔN is the yield under the photopeak; N_p is the projectile beam intensity (s⁻¹); N_n is the number of target nuclei (in 1/cm² units); t_1 is the irradiation time; t_2 is the time of exposure between the end of the irradiation and the beginning of the measurement; t_3 is the time measurement; λ is the decay constant (s⁻¹); η is the intensity of γ -transitions; k is the total coefficient of γ -ray absorption in target and detector materials, and ϵ is the γ -ray-detection efficiency.

If the yield of a given isotope receives a contribution from the β^\pm -decay of neighboring unstable isobars, the cross section calculation becomes more complicated [15]. If the formation probability for the parent isotope is known from experimental data or if it can be

estimated on the basis of other sources, then the independent cross sections of daughter nuclei can be calculated by the relation:

$$Y_B = \frac{\lambda_B}{(1 - \exp(-\lambda_B t_1)) \exp(-\lambda_B t_2) (1 - \exp(-\lambda_B t_3))} \times \left[\frac{\Delta N}{N_\gamma N_n k \epsilon \eta} - Y_A f_{AB} \frac{\lambda_A \lambda_B}{\lambda_B - \lambda_A} \left(\frac{(1 - \exp(-\lambda_A t_1)) \exp(-\lambda_A t_2) (1 - \exp(-\lambda_A t_3))}{\lambda_A^2} - \frac{(1 - \exp(-\lambda_B t_1)) \exp(-\lambda_B t_2) (1 - \exp(-\lambda_B t_3))}{\lambda_B^2} \right) \right], \quad (2)$$

where the labels A and B refer to the parent and the daughter nucleus, respectively; the coefficient f_{AB} specifies the fraction of A nuclei decaying to a B nucleus (this coefficient gives the information of how much the β -decay affects our data; and $f_{AB} = 1$ is when the contribution from the β -decay corresponds to 100%); and ΔN is the total photo peak yield associated with the decays of the daughter and parent isotopes. The effect of the forerunner can be negligible in some limit cases, for example, in the case where the half-life of the parent nucleus is very long, or in the case where the fraction of its contribution is very small. In the case when parent and daughter isotopes could not be separated experimentally, the calculated cross sections are classified as cumulative (C).

The yield of fission fragment production of Ta induced by photon beams with bremsstrahlung energy $E_{\gamma-max} = 50$ and 3500 MeV are presented in Table I. In total, for the two energies measured, 61 yields were calculated for the fragment mass region $70 < A < 100$ u. The quoted uncertainties in the experimental yields are from the contributions of the statistical uncertainty (≤ 2 -3%), uncertainty in the target thickness ($\leq 3\%$), and uncertainty in the detector efficiency ($\leq 10\%$).

III. RESULTS AND DISCUSSION

From the production cross sections of the individual fragments we can construct the mass distribution (cross section of each isobar as a function of the mass number A). However, to obtain the cross section for each isobar with mass A it is necessary to estimate the cross sections of the isotopes not measured by the induced-activity method. The cross sections for these fragments can be obtained from the analysis of the charge distribution

of the corresponding isobar chain, i. e., the cross section as a function of Z for a given A . We assumed that the charge distribution can be well described by a Gaussian function characterized by the most probable charge, Z_P , (centroid of the Gaussian function) of an isobaric chain with mass A and the associate width, Γ_Z . Moreover, the assumption is made that the most probable charge, as well as the width of the charge distribution, vary linearly with the mass of the fission fragment. The following parametrization of the production yield as a function of the charge of the fission fragment is adopted [10]:

$$Y_{A,Z} = \frac{Y_A}{\Gamma_Z \pi^{1/2}} \exp\left(-\frac{(Z - Z_P)^2}{\Gamma_Z^2}\right), \quad (3)$$

where $Y_{A,Z}$ is the independent yield of the nuclide (Z, A) . The values Y_A stands for the total isobaric yield for given mass number A , Z_P is the most probable charge for the charge distribution of an isobars with mass number A and Γ_Z is the corresponding width parameter. The values Z_P and Γ_Z can be represented as slowly varying linear functions of the mass numbers of fission fragments:

$$Z_P = \mu_1 + \mu_2 A, \quad (4)$$

$$\Gamma_Z = \gamma_1 + \gamma_2 A, \quad (5)$$

where μ_1 , μ_2 , γ_1 and γ_2 are adjustable parameters determined by considering a systematic analysis of the fission fragments. The obtained values for these parameters are listed in Table II.

The mass distribution (isobaric yields) of fission fragments were then constructed by using the obtained values of Y_A for each isobar chain. These mass distribution for the two endpoint energies are plotted in Figs. 1 and 2, respectively. In these figures the experimental data points of the present work is represented by black square symbol. In Fig. 2 we also present the data from Ref. [16], which includes data from spallation process of Ta target fragmentation (^9Be , $^{22,24}\text{Na}$, and $A > 120$ u) at bremsstrahlung endpoint energy of 4 GeV (open circles).

As one can see in both Figs. 1 and 2, data in the expected mass region for fission fragments agree with the assumption of a symmetric mass distribution. This mass region was, then, fitted with a Gaussian shape function given by:

$$Y_f = \lambda_A \exp\left(-\frac{(A - M_A)^2}{\Gamma_A^2}\right) \quad (6)$$

where the parameter λ_A is the height, M_A is the average mass number, and Γ_A is the width of the Gaussian. These parameters were adjusted to the data and the obtained values are listed in the Table II as $(M_A)_{exp}$ and $(\Gamma_A)_{exp}$ for each endpoint energy. The width, as well as the height, of the mass distribution clearly increase with increasing photon energy. From the mean value of the mass distributions, we can also conclude that, on average, three and six mass units are emitted before and after fission at low and intermediate energies, respectively.

The integration over the Gaussian gives the experimental fission yields for each endpoint energies. Actually, to get the fission yields, we had to multiply the Gaussian integration by a factor 0.5, to take into account the double counting in the cross section due to the two fission fragments in each event. The experimentally determined values for fission yield for the endpoints energies 50 and 3500 MeV are $Y_f = 5.4 \pm 1.1 \mu\text{b}$ and $Y_f = 0.77 \pm 0.11 \text{ mb}$, respectively. The obtained measured total fission cross section at 50 MeV is in good agreement with the experimental value of $4.8 \pm 1.0 \mu\text{b}$ from Ref. [5] for photofission of ^{nat}Ta induced by 69 MeV monochromatic photons. For the higher energy photons (3500 MeV), the fission yield of the present work agrees well with the value of $0.64 \pm 0.06 \text{ mb}$ obtained for reaction of bremsstrahlung with endpoint energy of 3770 MeV on ^{181}Ta [17].

From our data we could also estimate the fissility defined as the ratio of fission cross section to total nuclear photoabsorption cross section ($D = Y_f/Y_{abs}$). To determine Y_{abs} it is necessary to take into account all possible decay channels of the excited nucleus being considered. The calculated fissility from our experimental fission cross section for the 50 MeV endpoint photons is $(0.23 \pm 0.05) \times 10^{-3}$ and for 3500 MeV is $(2.9 \pm 0.5) \times 10^{-3}$. Here we considered the photoabsorption cross section for the endpoint energy 3500 MeV by taking the average values of data above the quasi-deuteron region of photonuclear absorption from Refs. [3, 4, 8]. The fissility obtained for bremsstrahlung endpoint energy of 50 MeV is consistent with the trends calculated for photofission on ^{nat}Ta induced by monochromatic photons of 69 MeV [5] and for photofission of ^{181}Ta at an incident monochromatic photon energy of 100 MeV [7]. The fissility for the higher endpoint energy (3500 MeV) is in agreement with the systematics of fissilities as a function of Z^2/A for photofission reactions with Ta targets at intermediate energies up to 6.0 GeV [3]. A general trend of increasing fissility with increasing

photon energy for pre-actinide nuclei is consistent with what the results of a systematic investigation of fission induced by bremsstrahlung photons on *Bi, Pb, Ti, Au, Pt, Os, Re, Ta* and *Hf* target nuclei [18].

IV. CALCULATION WITH CRISP CODE

Calculations of fission cross sections within different models have provided good opportunities to estimate the validity of the various reaction mechanisms and to investigate characteristics of the processes taking place in reactions induced by different probes. Here we used the simulation code CRISP [19] to analyze our data. CRISP is a Monte Carlo model code to describe nuclear reactions that uses a two step process [20, 21]. First, an intranuclear cascade is simulated, following a time-ordered sequence of collisions in a many-body system [22–24]. When the intranuclear cascade finishes, the nucleus thermalizes and the competition between evaporation of nucleons and alpha-particles, and fission starts. This code was recently used to analyse fission reactions induced by protons and photons [25–27].

To analyze our data we pushed the code to simulate not only fission process but also spallation reaction, which might be an important reaction channel for proton and photon induced reaction at intermediate energies. The results of the CRISP calculations for both fission and spallation processes for our data on ^{181}Ta target, at two endpoint energies, are shown in Figs. 1 and 2. The results of the simulation for fission calculation, given by the dotted line, show clearly that the experimental distributions for both endpoint energies, taken into account only the intermediate mass (fission-fragment) region, can be well reproduced by one symmetric Gaussian curve. Both peak position and width of the distributions are well described by the CRISP model. We used for fission calculation the experimental parameters of the charge distribution listed in Table II. For the mass distribution at endpoint energy of 50 MeV, the small fluctuations in the calculation is due to a limitation in the statistics. Although 5×10^6 events were simulated, the resulting statistics for the fission of ^{181}Ta is low due to the small fission yields. The total fission yields for ^{181}Ta , as calculated by CRISP, are $5.3 \mu\text{b}$ and 0.81 mb at low and intermediate energies, respectively, which agree completely with our experimental values obtained by a Gaussian fitting procedure described in the previous section. The calculated mean mass of the high energy mass distribution, after evaporation of post-scission neutrons, is shifted to lower masses in comparison to the

experimental ones. It means that the yields of fission fragments grow faster for higher energy, because of the considerable amount of high-energy photons.

The results of the CRISP calculation for the spallation process are indicated by dashed lines in the Figs. 1 and 2. The black solid line in Fig. 2 indicates the sum of the calculated fission and spallation yields. As can be observed in Fig. 2, CRISP model does not give satisfactory results for the very light mass fragments region, and since nuclear fragmentation is not included in the model, this may be an indication that the fragmentation is relevant for explaining the fragment production in the mass range of 1-20 mass units.

CRISP calculations enables us to extract the fissility for 50 and 3500 MeV bremsstrahlung photon energies, which are 0.16×10^{-3} and 0.41×10^{-3} , respectively. A qualitative agreement is obtained between the experimental and calculated fissility value for the low energy photofission. For the high energy, the experimental fissility value is about one order of magnitude higher than the calculated value. A possible explanation for this is the fact that the total photon absorption yield is being overestimated by CRISP code due to a limitation of the model in taking into account all possible channels of decay of the excited target nucleus being considered.

Another source of information about the reaction dynamics that can be obtained from the simulation is the neutron production. The emission of neutrons starts already at the intranuclear cascade process with the pre-equilibrium production followed by the evaporation of neutrons from an equilibrated composite system. Both categories are referred to as pre-scission neutrons [28]. The post-scission neutrons are obtained when the system pass the scission point with neutron emission by the residual fragments. The neutron production can then have the following contributions:

- (i) from the composite system;
- (ii) during the transition of the composite system through the saddle-point configuration towards the scission point;
- (iii) during the neck rupture;
- (iv) from the accelerating fragments and;
- (v) after completion of their acceleration.

The contributions from (i), (ii) and (iii) are not distinguishable and are therefore considered as pre-scission neutrons. The contributions from (iv) and (v) are classified as post-

scission neutrons. With the CRISP model we can also obtain the average number of pre- and post-scission emitted neutrons. We present in Table III the average fissioning nucleus mass A_f , the average mass of fission fragment mass distribution after evaporation, A_{ff} , as well as the average number of pre- and post-scission neutrons. The sum of the two neutron emission contributions gives the total number of emitted neutrons, which can be compared with the experimental values in Table III. We observe a good agreement between the calculated and the experimental values for the low energy induced fission, showing that the theoretical predictions for the emission of neutrons are correct. However, for the higher energy (3500 MeV) the calculations of the neutron multiplicities from the excited ^{181}Ta nucleus is somewhat overestimated. The experimental neutron emission is 11 neutrons while the calculation gives 16 neutrons. Again we emphasize that the larger is the intranuclear cascade, and the evaporation/fission chains, more difficulty is the calculation. In this case, however, it is possible to observe that the main contribution to the disagreement between calculation and experiment comes from the fission fragment evaporation (post-scission neutrons). There are some points in the calculation which could lead to this discrepancies, but most of them are also present in the evaporation of the compound nucleus formed after the intranuclear cascade. There is one particular mechanism which is related only to the fragment evaporation, namely, the distribution of the excitation energy between the two fission fragments. In the CRISP model it is assumed that the excitation energy of the fissioning nucleus will be distributed to the two fragments proportionally to their masses, keeping the total excitation energy constant. Behind this assumption is the idea that there is no energy transfer in the scission process from microscopic to collective degrees of freedom. This is not necessarily true, and the large number of neutrons evaporated from the fragments may be an indication that part of the excitation energy may appear as collective motion of the fragments. We are working on this issue to improve the simulation code CRISP, but we can say that the present analysis with the CRISP code already indicates that our theoretical model gives a good description of the dynamical process taking place inside the nucleus during reactions at intermediate energies.

V. CONCLUSION

In this work we present the results of the investigation of the induced fission of ^{181}Ta nucleus by bremsstrahlung photon beams with endpoint energies of 50 and 3500 MeV. Photofission yields have been measured taking advantage of the induced-activity method in an off-line analysis. The absolute photofission yields have been determined for the two very different energy regimes taking into account the photon spectrum measured. Photofissility values were subsequently deduced for each endpoint energy of photons. The obtained total fission yields and fissility values have been found to agree quite well with the values obtained from the measurement at 69 and 3770 MeV of incident photon energies. An analysis of the charge and mass distribution of fission fragments from ^{181}Ta target have been performed with the CRISP code. The comparison between calculated parameters for ^{181}Ta target and the experimental data has shown that the CRISP model gives a good description of the main characteristics of the reaction under investigation at the two endpoint energies (50 and 3500 MeV). The small disagreement between experimental and calculated values was found for the neutron evaporation from the hot fission fragments. We argue that this problem can be related to the transfer of energy from microscopic to collective degrees of freedom in the fissioning system, which is being improved in the CRISP code.

Acknowledgment

G. Karapetyan is grateful to Fundação de Amparo à Pesquisa do Estado de São Paulo (FAPESP) 2011/00314-0 and 2014/00284-1, and also to International Centre for Theoretical Physics (ICTP) under the Associate Grant Scheme. A. D. and V. G. acknowledges the support from CNPq under grant 305639/2010-2 and 302969/2013-6, respectively.

-
- [1] T. Methasiri and S. A. E. Johansson, Nucl. Phys. A **167**, 97 (1971).
 - [2] I. Kroon and B. Forkman, Nucl. Phys. A **197**, 81 (1972).
 - [3] D. A. De Lima, J. B. Martins and O. A. P. Tavares, IL Nuovo Cim. A **103**, 701 (1990).
 - [4] V. Emma, S. Lo Nigro and C. Milone, Nucl. Phys. A **257**, 438 (1976).

- [5] O. A. P. Tavares, J. B. Martins, E. de Paiva *et al.*, J. Phys. G: Nucl. Part. Phys. **19**, 805 (1993).
- [6] J. B. Martins, E. L. Moreira, O. A. P. Tavares *et al.*, IL Nuovo Cim. A **101**, 789 (1989).
- [7] M. L. Terranova, O. A. P. Tavares, G. Ya. Kezerashvili *et al.*, J. Phys. G: Nucl. Part. Phys. **22**, 511 (1996).
- [8] M. L. Terranova, G. Ya. Kezerashvili, A. M. Milov *et al.*, J. Phys. G: Nucl. Part. Phys. **24**, 205 (1998).
- [9] E. de Paiva, O. A. P. Tavares, M. L. Terranova, J. Phys. G: Nucl. Part. Phys. **27**, 1435 (2001).
- [10] M. C. Duijvestijn, A. J. Koning *et al.*, Phys. Rev. C **59**, 776 (1999).
- [11] U. L. Businaro and S. Gallone, Nuovo Cimento **1**, 629 (1955).
- [12] A. Deppman, S. B. Duarte, G. Silva *et al.*, J. Phys. G **30**, 1991 (2004).
- [13] K. Masumoto, T. Kato, and N. Suzuki, Nucl. Instrum. Methods Phys. Res. **157**, 567 (1978).
- [14] N. A. Demekhina and A. S. Danagulyan, Yad. Fiz. **24**, 681 (1976) [Sov. J. Nucl. Phys. **24**, 355 (1976)].
- [15] H. Baba, J. Sanada, H. Araki *et al.*, Nucl. Instrum. Methods A **416**, 301 (1998).
- [16] K. A. Amroyan, S. A. Barsegyan, N. A. Demekhina, Sov J. Nucl. Phys. **56**, 4 (1993).
- [17] G. A. Vartapetyan, N. A. Demekhina, V. I. Kasilov, *et al.*, Sov J. Nucl. Phys. **14**, 37 (1972).
- [18] Yu. N. Ranyuk and P. V. Sorokin, J. Nucl. Phys. (USSR) **5**, 37 (1967) (Engl. Transl. Sov J. Nucl. Phys. **5**, 26 (1967)).
- [19] A. Deppman, O. A. P. Tavares, S. B. Duarte, *et al.*, Comp. Phys. Comm. **145**, 385 (2002).
- [20] A. Deppman, O. A. P. Tavares, S. B. Duarte, *et al.*, Phys. Rev. C **66**, 067601 (2002).
- [21] A. Deppman, O.A.P. Tavares, S. B. Duarte, *et al.*, Nucl. Instr. Meth. B **211**, 15 (2003).
- [22] A. Deppman, S. B. Duarte, G. Silva *et al.*, J. Phys. G: Nucl. Part. Phys. **30** 1991 (2004).
- [23] T. Kodama, S. B. Duarte, K. C. Chung, and R. A. M. S. Nazareth, Phys. Rev. Lett. **49**, 536 (1982).
- [24] M. Goncalves, S. de Pina, D. A. Lima *et al.*, Phys. Lett. B **406**, 1 (1997).
- [25] A. Deppman, *et al.*, Phys. Rev. C **88**, 024608 (2013).
- [26] A. Deppman, E. Andrade-II, V. Guimarães, G. S. Karapetyan, and N. A. Demekhina, Phys. Rev. C **87**, 054604 (2013).
- [27] A. Deppman, *et al.*, Phys. Rev. C **88**, 064609 (2013).
- [28] M. Strecker, R. Wien, P. Plischke, and W. Scobel, Phys. Rev. C **41**, 2172 (1990).

TABLE I: Yields of fission fragments measured for the reaction with photons at $E_{\gamma-max}=50$ and 3500 MeV on ^{181}Ta target.

Element	Type	Yield, $\mu\text{b}/\text{eq. q.}$	
		$E_{\gamma-max}=50$ MeV	$E_{\gamma-max}=3500$ MeV
^{59}Fe	C	-	≤ 10.0
^{64}Cu	I	-	12.0 ± 2.0
^{65}Zn	C	-	18.0 ± 5.0
^{69m}Zn	I	-	21.0 ± 3.0
^{71m}Zn	C	-	22.0 ± 2.0
^{72}Zn	C	0.13 ± 0.02	23.0 ± 3.0
^{72}Ga	I	-	≤ 7.2
^{73}Ga	C	0.14 ± 0.02	25.0 ± 3.7
^{74}As	I	0.20 ± 0.03	20.0 ± 4.0
^{75}Se	C	-	29.0 ± 4.0
^{76}As	I	0.20 ± 0.03	22.0 ± 3.0
^{77}Ge	C	0.20 ± 0.03	29.0 ± 4.0
^{77}Br	I	-	≤ 5.0
^{78}Ge	C	0.25 ± 0.04	22.0 ± 2.2
^{78}As	I	-	15.0 ± 2.3
^{82}Br	I	-	23.0 ± 4.0
^{84}Br	C	0.40 ± 0.06	31.0 ± 6.0
^{84}Rb	I	-	4.0 ± 0.7
^{84m}Rb	I	-	≤ 5.0
^{85m}Sr	C	-	27.0 ± 5.0
^{86}Rb	I	0.36 ± 0.05	15.0 ± 3.0
^{87}Kr	C	0.45 ± 0.07	33.0 ± 3.3
^{87}Y	C	-	≤ 8.8
^{88}Kr	C	0.40 ± 0.06	30.0 ± 6.0
^{88}Y	I	-	≤ 7.0
^{88}Zr	C	-	≤ 10.0
^{90m}Y	C	-	41.0 ± 6.0
^{91}Sr	C	0.38 ± 0.06	35.0 ± 7.0
^{91m}Y	C	-	≤ 9.0
^{92}Sr	C	0.36 ± 0.05	33.0 ± 7.0
^{92}Y	I	-	≤ 7.0
^{93}Y	C	0.29 ± 0.04	36.0 ± 6.0
^{95}Zr	C	0.40 ± 0.06	34.0 ± 5.0
^{95m}Nb	I	-	9.0 ± 1.4
^{96}Nb	I	-	32.0 ± 5.0
^{96}Tc	I	-	≤ 4.0
^{97}Zr	C	0.28 ± 0.04	27.0 ± 5.4
^{99}Mo	C	0.27 ± 0.04	29.0 ± 6.0
^{100}Pd	C	-	13.0 ± 2.6
^{102}Rh	C	-	22.0 ± 5.0
^{103}Ru	C	0.15 ± 0.03	25.0 ± 5.0
^{105}Ru	C	0.15 ± 0.03	13.0 ± 2.6
^{105}Rh	I	-	≤ 4.0

TABLE II: Parameters values obtained for the mass and charge distributions for ^{181}Ta target at the endpoint energies of 50 and 3500 MeV.

Parameter	50 MeV	3500 MeV
$(\lambda_A)_{exp}$	0.00040 ± 0.00001	0.0410 ± 0.0002
$(\lambda_A)_{cal}$	0.0004	
$(M_A)_{exp}$	88.0 ± 0.6	85.0 ± 0.6
$(M_A)_{cal}$	87.9	82.5
$(\Gamma_A)_{exp}$	14.39 ± 0.20	23.5 ± 0.3
$(\Gamma_A)_{cal}$	15.0	
$(\mu_1)_{exp}$	1.69 ± 0.11	0.779 ± 0.046
$(\mu_1)_{cal}$	1.690	
$(\mu_2)_{exp}$	0.397 ± 0.002	0.420 ± 0.001
$(\mu_2)_{cal}$	0.397	
$(\gamma_1)_{exp}$	0.590 ± 0.007	0.590 ± 0.003
$(\gamma_1)_{cal}$	0.59	
$(\gamma_2)_{exp}$	0.0050 ± 0.0009	0.0050 ± 0.0004
$(\gamma_2)_{cal}$	0.0050	

TABLE III: Calculated and experimental parameters obtained for the mass distribution: mean mass of the fissioning nucleus $[(A_f)_{cal}]$ after evaporation of pre-scission neutrons from the compound nucleus; mean mass of the fissioning nucleus $[(A_{ff})_{cal}]$ after evaporation of post-scission neutrons from fragments; experimental mean mass of the fissioning nucleus $[(A_{ff})_{exp}]$, which includes both type of evaporated neutrons; number of pre- and post-scission neutrons, evaporated from the excited nucleus, fission cross sections.

Parameter	50 MeV	3500 MeV
$(A_{ff})_{exp}$	176.0 ± 0.9	170.0 ± 0.9
$(A_{ff})_{cal}$	175.8	165.0
$(A_f)_{cal}$	180.4	178.3
(pre-scission neutrons) $_{cal}$	0.6	2.7
(post-scission neutrons) $_{cal}$	4.6	13.3
(evaporated neutrons) $_{exp}$	5.0 ± 4.0	11.0 ± 1.2
(fission cross section) $_{exp}$	$5.4 \pm 1.1 \mu\text{b}$	$0.77 \pm 0.11 \text{ mb}$
(fission cross section) $_{cal}$	$5.3 \mu\text{b}$	0.81 mb

FIG. 1: Mass-yield distribution for photofission of ^{181}Ta at endpoint energy of 50 MeV. The present experimental data are shown by solid square symbol, the results of CRISP code calculation for fission is given by the dotted line curve, and for spallation by the dashed line curve.

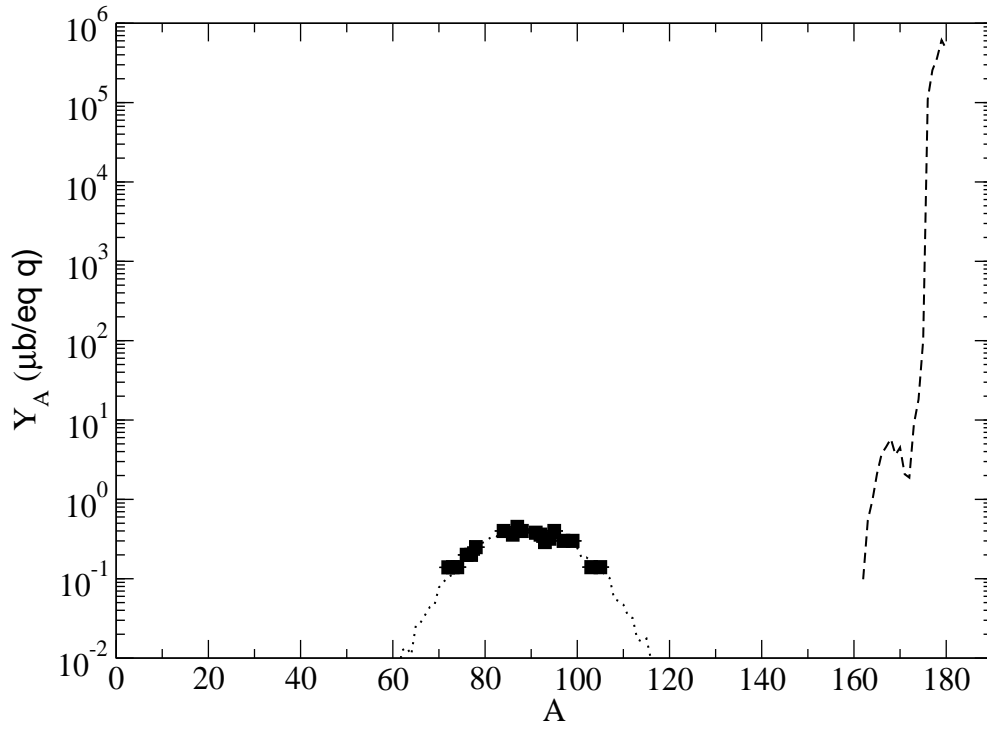


FIG. 2: Mass-yield distribuion of photofission of ^{181}Ta at endpoint energy of 3500 MeV. The present experimental data are shown by the solid square symbol. The open circle symbol correspond to data taken from Ref. [16] wich includes also spallation contribution. The results of the CRISP code calculation for fission is given by the dotted line, and for spallation by the dashed line curve. The black solid line indicates the sum of the calculated fission and spallation yields.

